university of groningen

faculty of science and engineering

Characterization of BaF_2 Detectors for Neutron Cross-Section Determination

Sergio Dharamraj

university of groningen / faculty of science and engineering

University of Groningen

Characterization of BaF_2 Detectors for Neutron Cross-Section Determination

Bachelor's Thesis

To fulfill the requirements for the degree of
Bachelor of Science in Physics
Faculty of Science and Engineering
University of Groningen

Performed at:

Energy and Sustainability Research Institute Groningen (ESRIG)

Sergio Dharamraj (S4292405)

First Examiner: Dr. Myroslav Kavatsyuk
Second Examiner: Prof. Nasser Kalantar-Nayestanaki

July 11, 2023

Contents

Abstract

The GELINA facility in Geel, Belgium is a neutron source renowned for its fast time resolution of 2ns [1]. Its GAINS spectrometer focuses on neutron inelastic cross-sections, with this process of scattering being a common occurrence in fission reactor cores. It currently consists of HPGe detectors, with remarkable energy resolutions. However, there has been interest in upgrading the spectrometer with the addition of detectors with relatively higher efficiences.

In this research, the suitability of the scintillator detector BaF_2 for neutron cross-section determination was characterized. Using the trapezoidal FIR energy filter approach, the energy resolutions at different energies were determined with ^{60}Co and ^{22}Na radioactive sources. The resolutions were then compared to literature values, followed by an analysis of the scaling behaviour with respect to the incident photon energy.

1 Introduction

Meeting energy demands, especially sustainably and efficiently, is a topic of great interest in modern times. There have been steady advances in renewable energy sources, but regardless, one other particular source of interest, is nuclear power, being both reliable and safe [2]. However, as with any power plant, minimizing risk and maximizing efficiency while maintaining safe functionality is desired. For the most part, a lot of this can be understood by better understanding neutron behaviour and their interactions with other materials that can be found within a reactor vessel. One establishment investigating this area of neutron interactions in the context of nuclear energy, is the GELINA-GAINS facility of the European Commission Joint Research Center in Geel, Belgium. GELINA, the Geel Linear Accelerator, is a pulsed white neutron source with a remarkably fast time resolution of 2ns [1]. GAINS, the Gamma Array for Inelastic Neutron Scattering, uses this neutron source to obtain information about, as the name suggests, inelastic neutron scattering [3]. More investigation into inelastic neutron scattering, being a very relevant process within nuclear reactors, would allow for better understanding and management of neutron economy within the reactor, especially for new Generation IV reactors such as the molten-salt thorium reactors [3].

Currently, the GAINS spectrometer consists of 12 high volume high purity germanium (HPGe) detectors, having been upgraded a few times from initially having two [1]. These semiconductor detectors have notable energy resolutions of e.g. 2.5 keV for the 1332 keV peak of ^{60}Co, which corresponds to a value of 0.188% [1]. However, compared to another common type of detector used for gamma detection, scintillators, the efficiency of HPGe detectors doesn't compare [4]. For example, the relative efficiency of NaI(Tl), a type of scintillator, at 500 keV is around 1.5x better than that of HPGe [5].

Thus, it might be of interest to include detectors of better efficiencies within the GAINS spectrometer. This project in particular will be concerned with another form of scintillator detector, namely Barium Flouride (BaF_2). In other words, this thesis will be concerned with characterizing BaF_2 detectors for neutron cross-section determination.

In terms of energy resolution, BaF_2 has been said to have a resolution of around 9.8% at 511 keV [6] and around 6.4% at 1.334 MeV (at room temperature) [7]. Recalling the efficiency that HPGe can achieve at the latter peak, the difference in resolution is obvious. Such a difference is primarily due to the detection mechanism of the detectors, being two very different processes. That being said, BaF_2 may be able to achieve better efficiencies, especially due to it's high density. However, due to time constraints, this thesis will only focus on probing and analyzing the energy resolutions achievable by BaF_2 crystals. Investigating the efficiencies can therefore be the focus of future work. Regardless, understanding the resolution is still relevant in the context of neutron cross-section determination, being the focus of the GAINS spectrometer.

2 Theory

Before diving into the investigation of this project's focus, it would be important to consider the following subsections to properly appreciate what is being investigated and why. This would allow for a more comprehensive understanding of the approach, as well as the results and the following interpretation of them.

2.1 Inelastic Neutron Scattering

As mentioned in the introduction, the GAINS spectrometer measures inelastic neutron scattering events. It was also mentioned that the current detectors used are HPGe detectors, which are detectors used for ionizing radiation. The reason that these detectors are used is that upon colliding with the stationary target, the neutron can inelastically scatter off of it, where the momentum difference translates to a kinetic energy difference accounted for by the excitation of particles in the target [8]. Upon de-excitation of these particles, the target nucleus emits a photon of corresponding energy, which is then detected by the HPGe detectors.

2.2 Scintillators

Scintillators are materials that absorb ionizing radiation and subsequently emit photons of relatively lower energy [8]. This property makes them very suitable for applications in experiments where gamma detection is required, like in nuclear physics. Compared to semiconductor detectors, such as HPGe detectors, scintillators tend to have on average relatively higher efficiencies with lower energy resolutions [4].

The reason that scintillating materials are able to subsequently emit lower-energy photons is due to the Stokes shift [8]. Upon electronic excitation to the conductance band from the valence band due to the incident photon, the electron configuration of the scintillating atom will compensate and adjust accordingly. This results in a smaller energy difference between the conductance and valence band once the excited electron de-excites. An example of this is visualized in the figure below.

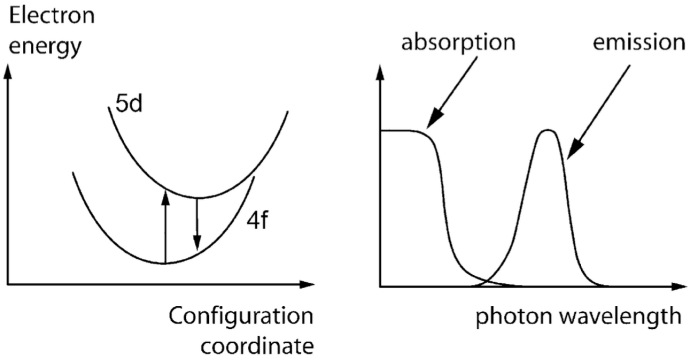

Figure 1: Visualization of the Stoke's shift corresponding to a longer emitted wavelength [8]

In the example above, an electron in the 4f shell is promoted to the 5d shell upon excitation. The Stokes shift then follows, when the electronic configuration adjusts for the now missing electron. This thus results in a longer wavelength, and thus lower energy, for the emitted photon relative to the absorbed one.

2.2.1 Barium Fluoride

Barium Fluoride (BaF_2) is a type of an inorganic scintillator with a high density of 4.88 g/cm^3 [9]. Having a high density is very beneficial when attempting to detect gamma rays, since having a higher density means that the atoms are more closely packed. This results in a higher probability of interaction of the photon with atoms of the detector, causing the detector to have relatively higher efficiencies.

As for output, undoped BaF_2 contains output pulses with two components: a fast component and a slow component. The fast component has a very fast decay time of 0.6 ns at wavelengths of around 220 nm, while accounting for 15% of the light yield, whereas the slow component has a much longer decay time of 630 ns at wavelengths of around 320 nm, accounting for 85% of the light yield [10]. It might be important to mention that these are the properties of specifically undoped BaF_2 crystals, as crystals can be doped with impurities to improve properties such as time resolution, combining the two components into one coherent output.

As mentioned in the introduction, the expected energy resolution for 511 keV is 9.8% and around 6.4% at 1.334 MeV (at room temperature). It is thus seen that the magnitude of energy resolution decreases as the incident photon energy increases. It can be further inferred that the energy resolutions for photons between and above these energies follow a relationship. This relationship will be explained more in depth in Section 2.4.1.

2.2.2 Photomultiplier Tubes

When earlier discussing scintillators, it is mentioned that they produce photons. However, in order to collect data, these must be converted into something more readable, such as an electric current.

Photomultiplier tubes (PMTs) are paired with scintillating crystals in order to convert the produced photons into electric signals. PMTs are designed to detect individual photons. Since a single photon results in the production of a single electron, the internal gain of the PMT should be very high in order to output a detectable signal.

The working principle of a PMT first begins with the incident photon hitting a photocathode, releasing photoelectrons [8]. These electrons then pass through a series of dynodes, multiplying the amount of electrons every time. In order for the electrons to continue to move towards and strike the dynodes, a high voltage must be supplied to the PMT, pointing from the cathode to the anode where the end current is read from. See the figure below for a visualization of this.

Usually, there are specific voltages and polarities suggested to supply to a given PMT. While making sure the correct polarity is supplied, the magnitude of the supplied voltage can vary. Although the timing properties of the PMT are optimized only when operated near the recommended voltage, other general properties such as linearity and relative signal-to-noise ratio are not seriously changed over wide ranges of voltage [11]. Thus, it is possible to supply a PMT with a voltage lower than recommended, while observing little change in behaviour. However, the voltage cannot be too low, as the performance sometimes can suffer at the lower voltages due to reduced gain at the critical first dynode [11].

2.3 Compton Scattering

There are three main ways that photons can interact with matter: the photoelectric effect, Compton scattering, or pair production [8]. The probability of each of these processes occurring depends on the energy of the incident photon. In the context of obtaining spectra for radioactive sources, Compton scattering within a PMT occurs regularly. This can manifest into structures in obtained spectra, as can be seen in the example spectrum below.

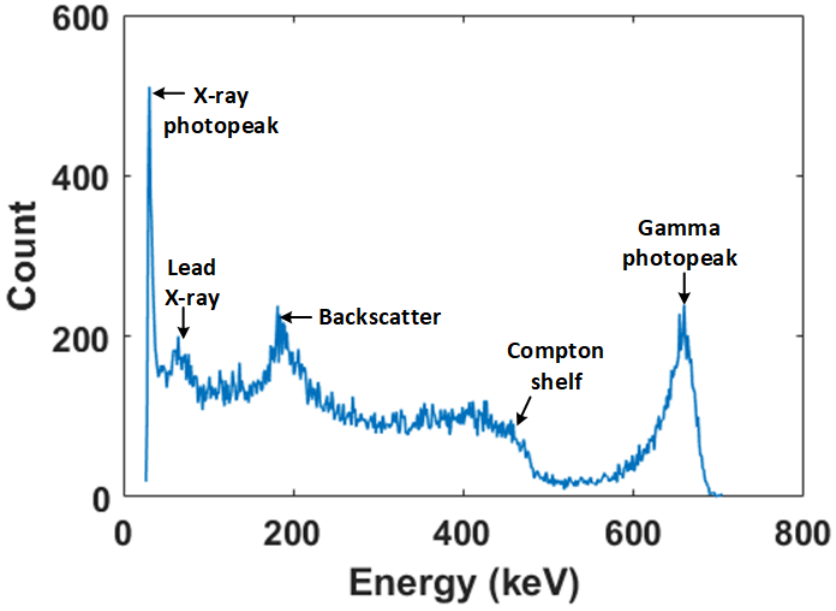

Figure 2: Spectrum for ^{137}Cs obtained by a Cadmium Zinc Telluride (CZT) detector showing various structures including the Compton shelf [12]

In the figure above, besides the expected photo peaks, there exist other structures including the Compton shelf, as well as a structure due to the backscattering of photons from the PMT.

2.4 Energy Resolution

The term energy resolution has been mentioned a couple of times already, but has never been discussed in detail. Often when attempting to obtain energy spectra with detectors, as opposed to a sharp peak at the explicit incident photon energy value, a Gaussian distribution about that energy is obtained. Therefore, the energy resolution obtained from the plot of an energy spectrum can be expressed as [13]:

$$\frac{\Delta E}{E} = \frac{FWHM}{mean} \tag{1}$$

where FWHM stands for the full width of the peak of interest at half maximum, and the mean represents the corresponding position of that peak, thus corresponding to the incident photon energy. Thus, when the magnitude of resolution is lower, e.g. the closer it is to zero, the resolution is considered to be better.

Additionally, as can be seen from the equation, the energy resolution is thus dependent on the incident photon energy.

2.4.1 Energy Resolution Photon Energy Relationship

Now that it is known that the energy resolution depends upon the photon energy, coupled with the fact that up until this point, the energy resolution was mentioned only for specific photon energies, this subsection will explain the exact relationship between the two values.

It is known that the resolution is a function of the FWHM, but the FWHM is also related to the standard deviation of a Gaussian distribution via [14]:

$$FWHM = 2.35\sigma \tag{2}$$

Additionally, the standard deviation of the Gaussian distribution is related to the statistical fluctuations in the number of photo-electrons, N_e, that are collected from the photocathode of the PMT via [14]:

$$\sigma = \sqrt{N_e} \tag{3}$$

Since N_e is proportional to the gamma energy [14], it can be said that:

$$\frac{FWHM}{mean} \propto \frac{\sqrt{E}}{E} = \frac{1}{\sqrt{E}} \tag{4}$$

$$\therefore Resolution \propto \frac{1}{\sqrt{E}} \tag{5}$$

Thus showing that for higher incident photon energies, the magnitude of the energy resolution decreases, meaning that the resolution improves. However, this is just a proportionality. The magnitude of the energy resolution does not exactly scale with photon energy via the relationship above. Thus, it was decided to introduce two more parameters in order to probe how exactly the magnitude of energy resolution scales with the incident photon energy. The parameters are: a scaling factor, C, and an offset factor, D. This gives the equation:

$$\frac{C}{\sqrt{E}} + D \tag{6}$$

where ideally $C > 1$, $D = 0$. C, the scaling factor, simply accounts for the scaling of the energy resolution values for which the inverse square root relationship follows more accurately. The offset however, is more relevant when investigating the plausibility of the experimentally obtained resolutions and/or the experimental approach. The closer the offset is to zero, the closer the energy resolutions obtained follow theoretical predictions. Thus, determining the offset factor is a useful consideration when investigating the energy resolution of a detector and how it scales with different incident photon energies.

3 Approach

3.1 Resolution-Energy Relationship

As previously mentioned, the area of interest for this thesis would be how the energy resolution of undoped BaF_2 detectors scales with an increase in the incident photon energy. In order to approach this, the detector was exposed to different radioactive sources with gamma radiation of known energies. It was then attempted to obtain a histogram of the energy spectrum of the sources.

Once the spectrum was obtained, the expected peaks were analyzed, determining the corresponding FWHM and mean values. These values were then used to obtain the energy resolution of the detectors at those energies. A plot of energy resolution against the energy of incident photons was then made to observe the relationship between the two.

3.2 Experimental Approach

This section will discuss more of the practicalities that were necessary to consider when approaching this problem experimentally. Firstly, the entire setup including whatever additional components were required will be explained, followed by how the detector output was processed and stored.

3.2.1 Experimental Setup

There were 3 available undoped BaF_2 scintillation detectors, which can be seen in Figure 3 below. Each detector contained 4 PMTs each, all acting as independent detectors, which was previously confirmed via an oscilloscope. This effectively means that there were 12 available detectors to work with.

(a) Detector 1 (b) Detector 2 (c) Detector 3

Figure 3: BaF_2 detectors used for data collection

The detectors consisted of XP4318/B photomultiplier tubes, equipped with VD123K voltage divider bases where the bias voltage and output signal cables could be attached.

Figure 4: The type of photomultiplier tube and voltage divider attached to the BaF_2 crystals in the detectors

Figure 5: Labelling for PMTs on the detectors

The labelling used for the PMTs in Figure 5 above will be used across all detectors and is how they will be referred to from now on.

In order for the detectors to function, high voltage must be supplied to the PMTs attached to the crystals. This was done using the CAEN SY 1527 Universal Multichannel Power Supply System.

Though the documentation for XP4318/B PMTs stated that the functional voltage is 2200V [15], pulses were produced for the voltage of 1000-1300V across the detectors. When trying to go higher than this for the first detector, being the detector that all of the approach settings were based upon, a pulse exhibiting ”ringing” behaviour was observed. This was the case especially when a radioactive source was introduced to the detector. The reason for this behaviour is either that some high oscillating signal is being produced somewhere in the circuit, or there was an overwhelming amount of photons being detected. In the latter case, this would mean that there are constantly single-photon pulses happening during the duration of what should be one pulse. Later on this was found to be due to light leaks in the detector, which will be discussed much further in Section 5.1.1.

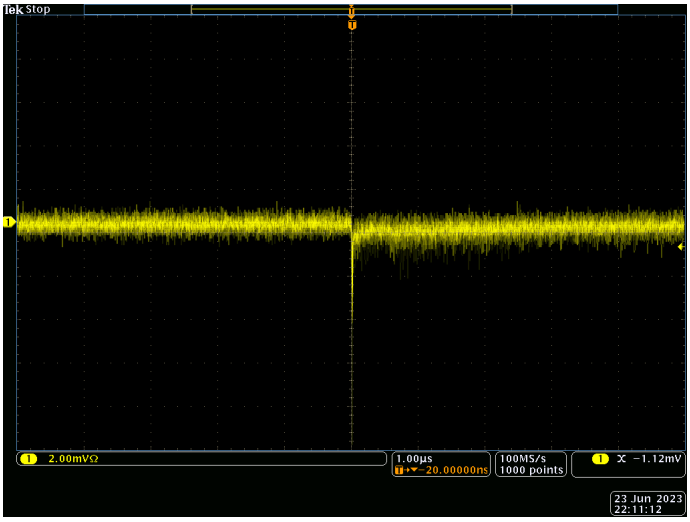

Figure 6: A signal produced by a BaF_2 detector supplied with too high voltage

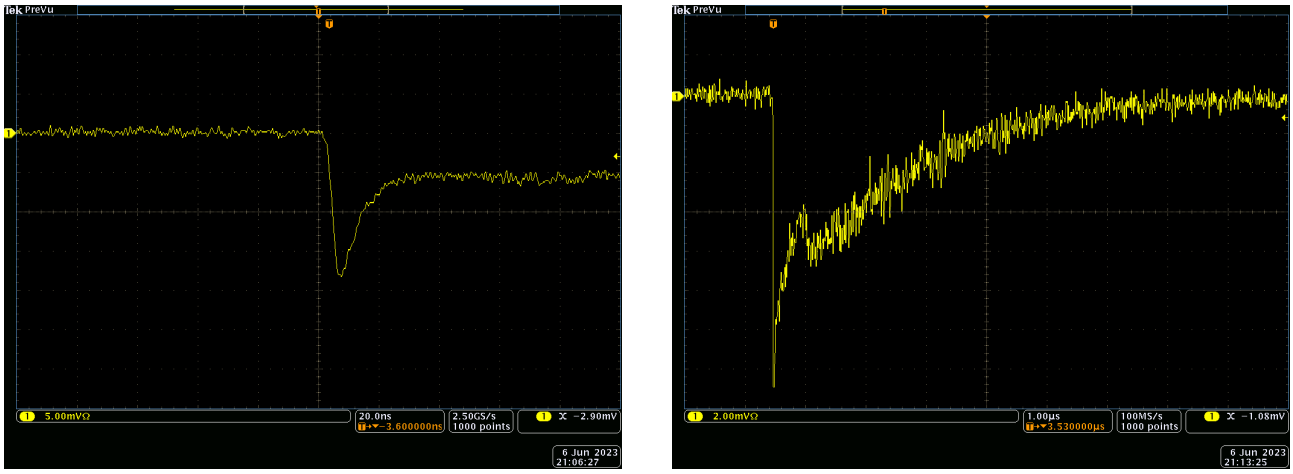

(a) Shorter time scale (20 ns intervals)

(b) Longer time scale (1 μs intervals)

Figure 7: Expected pulses produced by a BaF_2 detector

It might be worth mentioning that these pulses are induced by high energy cosmic ray energy deposition.

As can be seen in the expected pulse in Figure 7a, the time scale of the fast component is very short, being a value of < 20 ns wide for the entire pulse, and the amplitude of the output is around 15 mV.

This is important to consider, as the digitizer available was the SIS3316 digitizer. Using the SIS3316 digitizer comes with it's restrictions, namely the sample rate of 250 MHz and the maximum input voltage restriction of 5V [16]. This poses a slight problem since, as was seen previously in Figure 7, the typical output lies in the order of magnitude of 10s of millivolts with a decay time of a few nanoseconds. Both of these problems can be resolved by introducing the ORTEC 474 Timing Filter Amplifier (TFA) between the PMT and the digitizer. This was set to amplify the signals by x180-x285, depending on the detector, and set to integrate over every 50 ns.

A full schematic of the setup can be seen in the figure below.

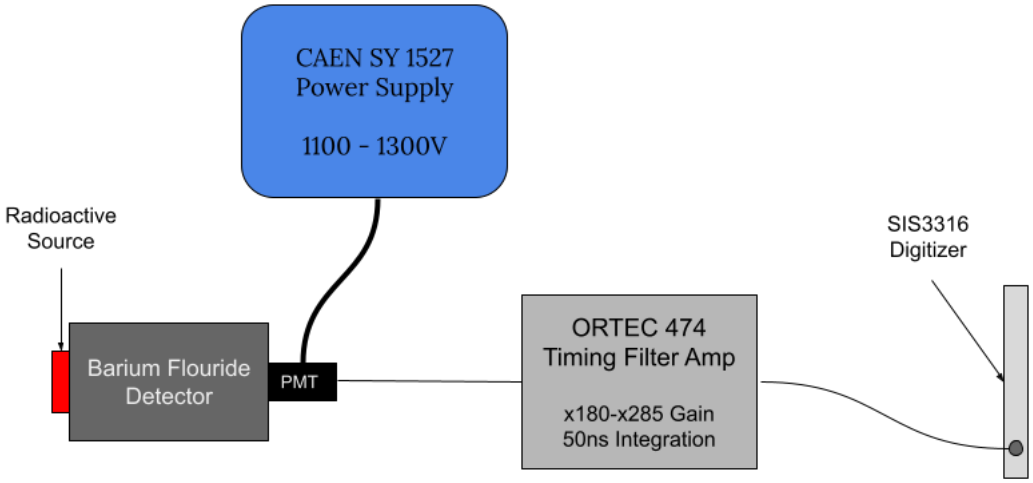

Figure 8: Schematic of setup for BaF_2 Characterization

The sources used for this investigation were a ^{60}Co source, emitting gamma rays with energies of 1.173 and 1.332 MeV, and a ^{22}Na source, emitting gamma rays with energies of 511 keV and 1.274 MeV [17]. When taking measurements, these sources were placed directly in front of the detectors.

3.2.2 Method of Data Collection

Besides being able to receive digital signals, the signals must also be analysed sufficiently in order to obtain histograms displaying the energy spectra for a given radioactive source.

Using the software intended for use of the SIS3316 digitizer, the detector outputs were viewed and stored. An example of what a typical pulse would look like can be seen in the figure below.

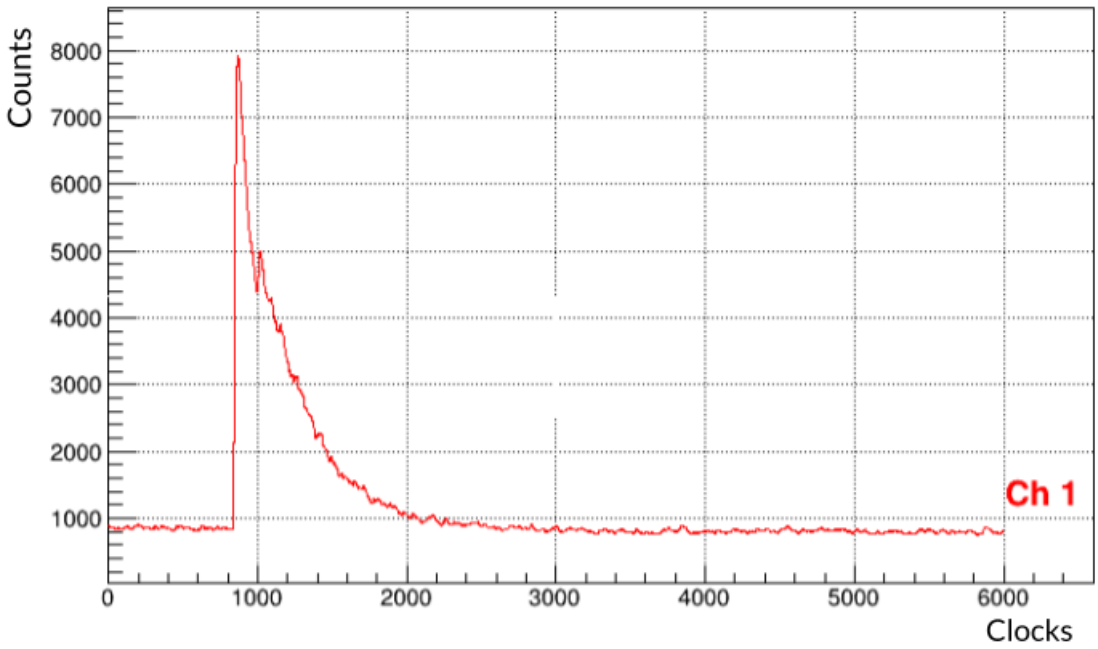

Figure 9: ”ADC” graph showing a pulse corresponding to a cosmic ray detection by a BaF_2 detector

The ADC histogram above shows arbitrary units proportional to voltage, and therefore energy, in the vertical axis, and channels called ”clocks” in the horizontal one, being proportional to time. This thus shows the shape of the pulses received and gives an idea as to the energy of the photon detected by the detector, indicated by the height of the pulse. There also exists an offset of +800 in the vertical axis. This offset from 0 exists as, being a histogram, the graph is incapable of displaying negative values. Negative values would then be displayed as values below this offset. For the purposes of this report however, this is unimportant as only positive pulses will be of interest.

Since this pulse contains information about the gamma rays detected, how this information is stored and plotted is important. The approach chosen was to use the Trapezoidal Finite Impulse Response (FIR) Energy Filter [16]. This generates two ”moving windows” separated by an adjustable gap value, across the pulse seen in the ADC histogram, where the section of the pulse within the windows are integrated. The difference between these two windows is calculated, with the maximum integration value for a given pulse then being stored. This maximum value can be seen in another graph, which can be seen below.

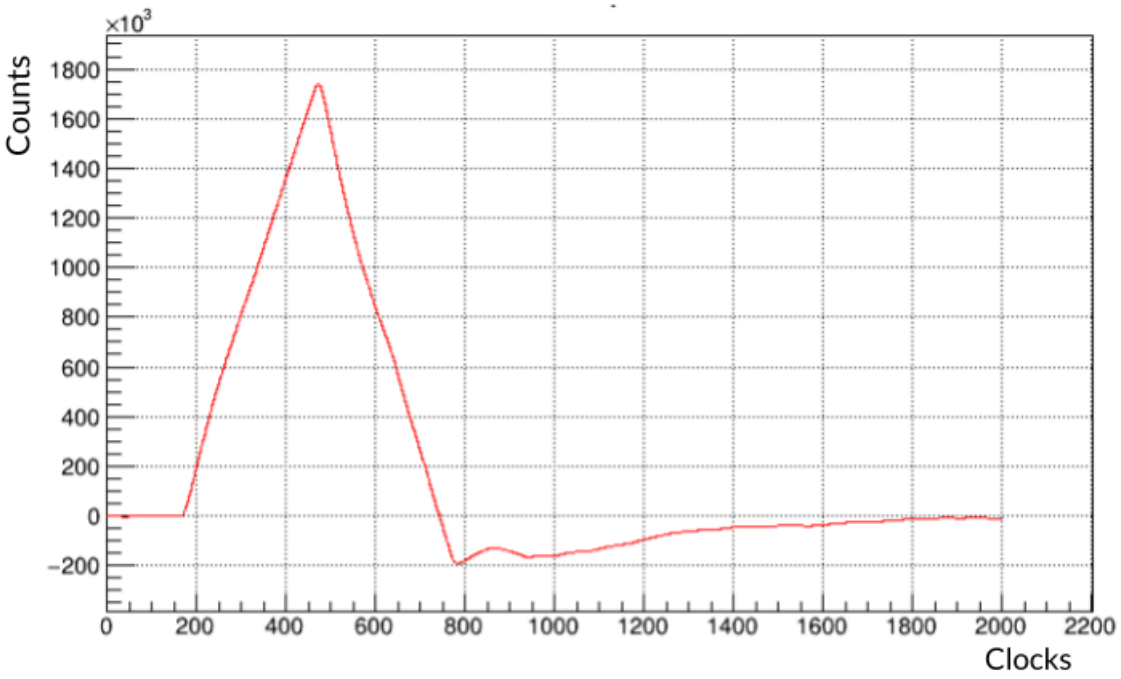

Figure 10: Moving average window (MAW) histogram corresponding to the Trapezoidal FIR Energy Filter

This MAW histogram consists of similar axes as the ADC histogram, where it can be seen that there is a triangle shape, with the tip corresponding to the peak value stored, followed by a decay tail that resolves to zero.

The width of the windows must not be too small as it must encompass enough information of the pulse, and it cannot be too big otherwise more noise will be included in the integration, both reducing the energy resolution of the histograms that will eventually be plotted with the stored data. The gap between them must also not be too large, so as not to exclude the beginning of the pulse. Lastly, the negative difference between the windows once it passes through the pulse when the first window is now higher than the second, must not produce a negative contribution to the MAW and stored data. This can be corrected by taking the pulse decay time into account.

There exist various parameters that can be tuned to idealize the stored information. The first parameter, called the ”Energy Peaking Value”, dictates the width of the moving windows across the ADC histogram. The second parameter, called the ”Energy Gap”, dictates the value of the gap between both windows, which also possibly results in a plateau in the middle of the triangle observed in the MAW, and hence why the filter is called ”Trapezoidal”. The last two parameters of relevance dictate if and how the tail seen in the MAW histogram resolves to zero. These values depend on the pulse decay time specific to the crystal.

All of the data seen in this thesis were taken for a 5 minute measurement using an Energy Peaking Value of 300, and an Energy Gap of 5. Multiple test measurements were taken for differing values, but the best resolution was obtained for these settings. Since, as seen in Figure 9, the pulse lasts for about 1000-1200 clocks, a width of 300 for the windows was thus the width for which the most noise is excluded in the integration, while still registering the pulse. For the decay time values, however, they are set once the decay time is known. Thus, they did not need further adjustment.

4 Results

The most straightforward way to measure the performance of a detector is to analyze the measured distribution of energy deposition from the different sources. These resulted in histograms, which will be shown and discussed in this section. These histograms were plotted using ROOT. The following sections show what types of histograms were obtained and how they were adjusted in order to display the energy spectra sufficiently enough for analysis.

4.1 Histograms Produced

The following figure shows an example of the histogram generated when plotting the data obtained when taking a background measurement.

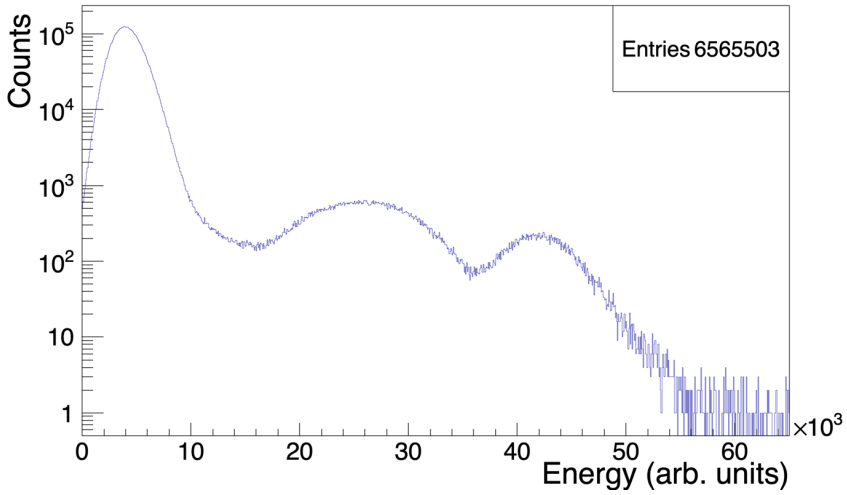

Figure 11: Histogram for a 5 minute background measurement taken by the Top Right PMT of Detector 1 (D1TR)

Firstly, it can be seen that the horizontal axis is in arbitrary units as opposed to electronvolts. This, however, is not a problem as the shape of the spectrum is what is important, with the relationship between the mean, standard deviation and the FWHM also being conserved in it. Upon later comparing the background measurement to a measurement taken with a source, the appearance of new peaks would indicate which arbitrary units correspond to photons of known energy.

In order to observe the various structures visible in the obtained spectrum, the vertical axis had to be set to a logarithmic scale. The main reason for this was the significant peak present in the lower end of the spectrum. This peak arises due to electronic noise being registered as pulses. The noise could be excluded by setting the pulse detection trigger threshold for the digitizer at a higher value. However, for some cases this was set lower due to reasons that will be discussed later.

As for the other two peaks, these are due to natural background radiation present which is picked up by the detector. For example, the peak seen towards the middle of the spectrum, between around 20,000 and 30,000 arbitrary energy units, is due to the presence of natural ^{40}K present in soil. ^{40}K emits photons with energy of 1.46 MeV [18]. This is known since, even with the arbitrary units, they can be compared to the position of the ^{60}Co peaks of known energy in the figure later on.

It may also be important to note that the binning of the histograms are adjusted in order to make the peaks more clear and visible. For the most part it will be kept constant across the histograms, but some might appear more clearly with a lower amount of bins than others. A consequence of this would be potential variations in the counts when comparing peaks of different histograms.

The figure below shows an example of the histogram obtained when taking a measurement with a ^{60}Co radioactive source.

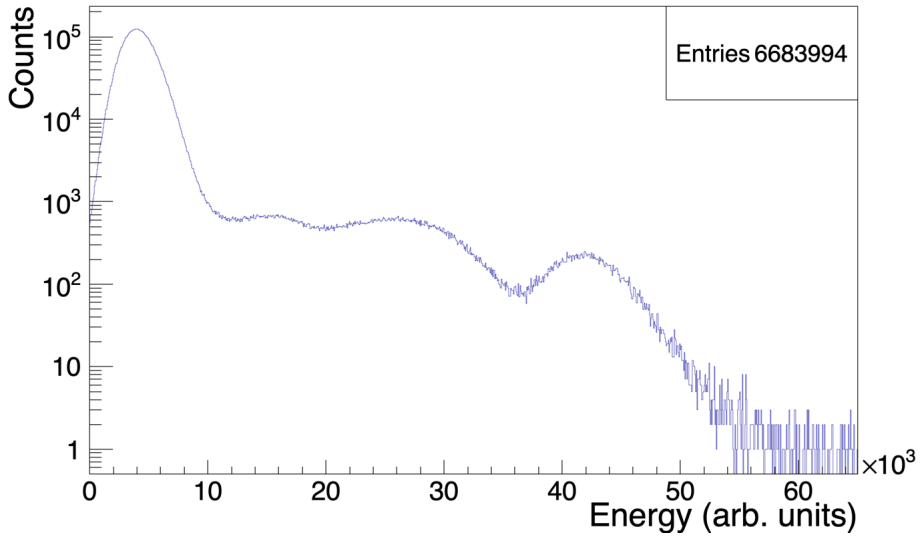

Figure 12: Histogram for a 5 minute measurement with ^{60}Co source taken by D1TR

As can be seen, the spectra looks quite similar, except for a new visible peak between 10,000 and 20,000 arbitrary energy units in the horizontal axis. It can also be seen that the entry count is noticeably higher due to the presence of the source. In order to obtain the energy spectrum of purely the ^{60}Co source however, the background measurement must be subtracted.

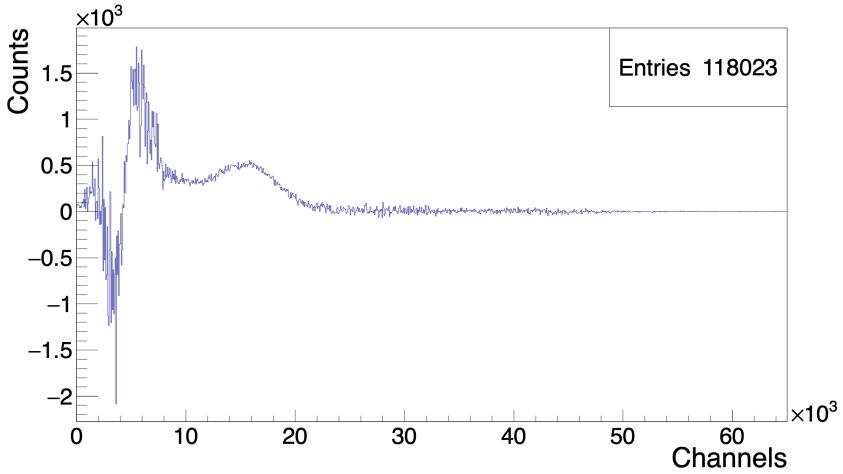

Figure 13: Histogram of a 5 minute measurement with a ^{60}Co source with background subtracted for D1TR

Once the background is subtracted, it can be seen that a linear scale can now be used in the vertical axis. This is because most of the electronic noise that caused the significant peak is of course common between the background and source measurements.

Something very prominent in Figure 13 above is the large negative peak seen in the lower channels. Due to the relatively long processing time of the digitizer, being in the order of magnitude of μs per pulse, and having a high-intensity source, less background noise counts were counted, resulting in this negative spike at the beginning of the subtracted histograms. From now on, this section will be cropped out in order to better see the peaks produced by the source, and also because this part doesn't affect the area of the spectrum that is of interest. However, once again, this could be avoided by increasing the trigger threshold of the digitizer.

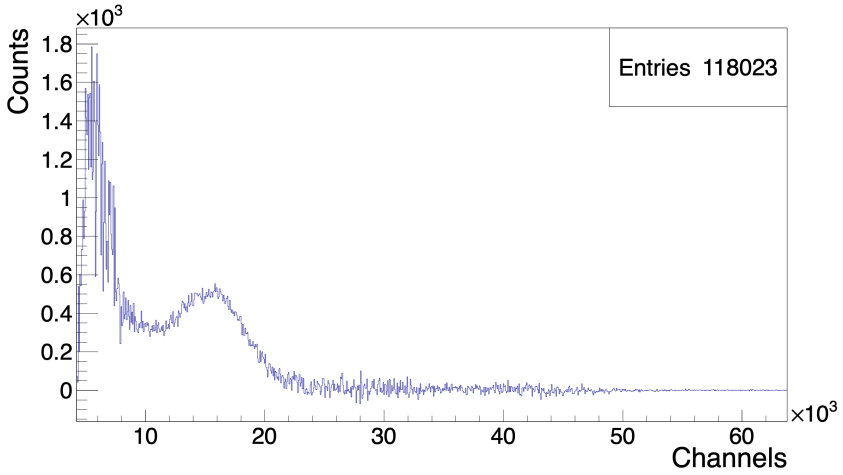

Figure 14: Cropped histogram of a 5 minute measurement with a ^{60}Co source with background subtracted for D1TR

After cropping the spectrum, it is easier to observe that only one Gaussian-resembling peak is visible. Recalling that ^{60}Co has two prominent peaks very close in energy, 1.173 and 1.332 MeV, it can be seen that the resolution is not sufficient enough to resolve both peaks. This was the case for all of the various PMTs across all 3 detectors, even for the best obtained spectrum for the ^{60}Co source, which can be seen in Appendix A. Thus, histograms using a ^{22}Na source will be shown as of this point, due to the presence of the very distinct peaks at 511 keV and 1.274 MeV.

4.1.1 Obtained ^{22}Na Source Spectra

Though the same digitizer settings were used across all 12 PMTs, different spectrum shapes were obtained for the ^{22}Na source. See the figures below for the three main shapes observed across the obtained spectra.

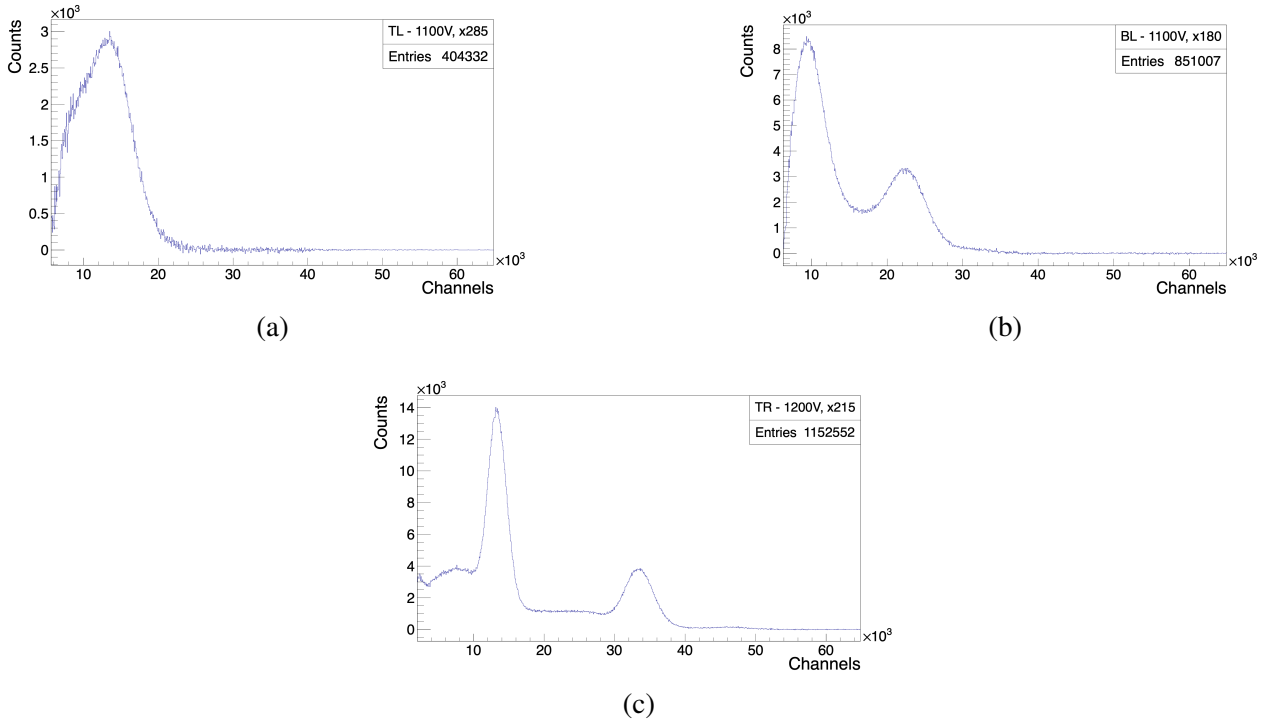

(a) (b)

(c)

Figure 15: Main background-subtracted energy spectra shapes for a ^{22}Na source obtained across all BaF_2 detectors

Firstly, in Figure 15a, it can be seen that there exists only one peak, with it being blended into the background. Upon comparison with the other spectra obtained, it can be see that the amount of counts of the visible peak corresponds to that of the 1.274 MeV peak of ^{22}Na. It appears that the PMT is not able to amplify the photon pulses outside of the order of magnitude of the background noise. This is not a matter of gain applied by the TFA, as multiple measurements were taken for different levels of gain, but all resulted in the same shape.

Secondly, in Figure 15b, the spectrum shows a true 1.274 MeV peak, but with the 511 keV peak being blended into the noise instead. Again, as was for the previous case, this could be a matter of the internal gain of the PMT. However, this can also occur when there exists an imperfect optical seal between the crystal and PMT.

Lastly, in Figure 15c, the best obtained spectrum shape can be seen. Here, both the 511 keV and the 1.274 MeV peaks can be observed, including some Compton effects in the lower end behind the 511 keV peak. In some cases, even the sum peak is visible. See Appendix B for these spectra.

4.2 Energy Resolutions

In order to obtain the energy resolutions, the means and standard deviations, sigma, or full-width half maximums (being related) must be known.

For spectra where the peaks were clearly visible and contained Compton effects that are expected, such as those of the shape in Figure 15c, the background was fitted alongside the peak. Examples of these fittings can be seen in the figures below.

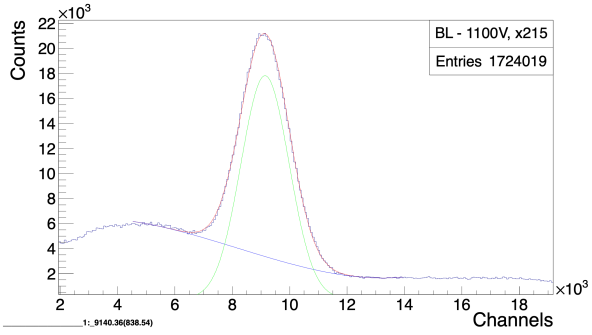

(a) 511 keV

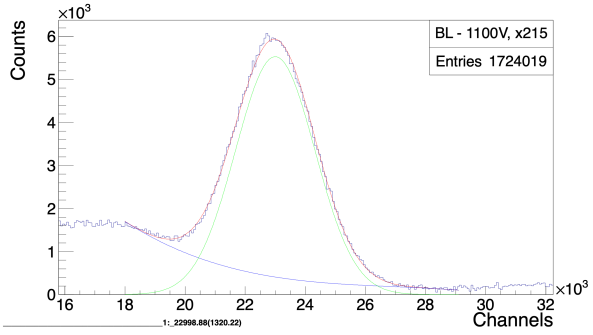

(b) 1.274 MeV

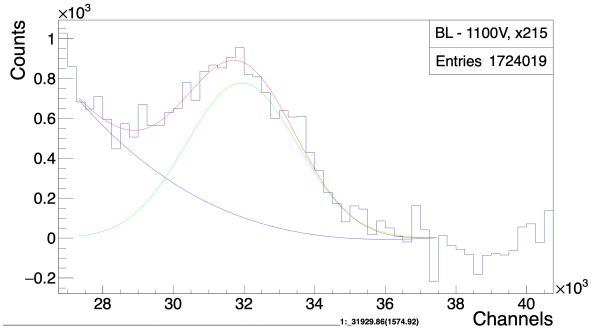

(c) Sum of 511 keV & 1.274 MeV

Figure 16: Examples of fitting peaks with background

As can be seen in the figures, the red line is the fraction of the spectrum where the function is being fitted, with the green line being the contribution of the actual photon of known energy, and the blue line being the background, mostly due to Compton scattering. For the code used, the background had to be plotted according to a certain function. The function chosen to predict this background behaviour was a third-order polynomial. Thus, the blue lines correspond to third-order polynomial functions, namely the section of the function containing the critical points. This is important as in Figure 16a, it can be seen that the fitted background function contains an inflection point.

For the peaks that were not very clear, e.g. blended into the background, or that contained a background that could not be predicted well, such as the case is with Compton effects, the peak could not be fitted properly with the background following a specific function. Thus, a simple Gaussian fit was done, where two points on the peak were first selected. This was done to at least obtain some information and idea of the energy resolution for these lower-resolution peaks. An example of a peak fitted with this approach can be seen in the figure below.

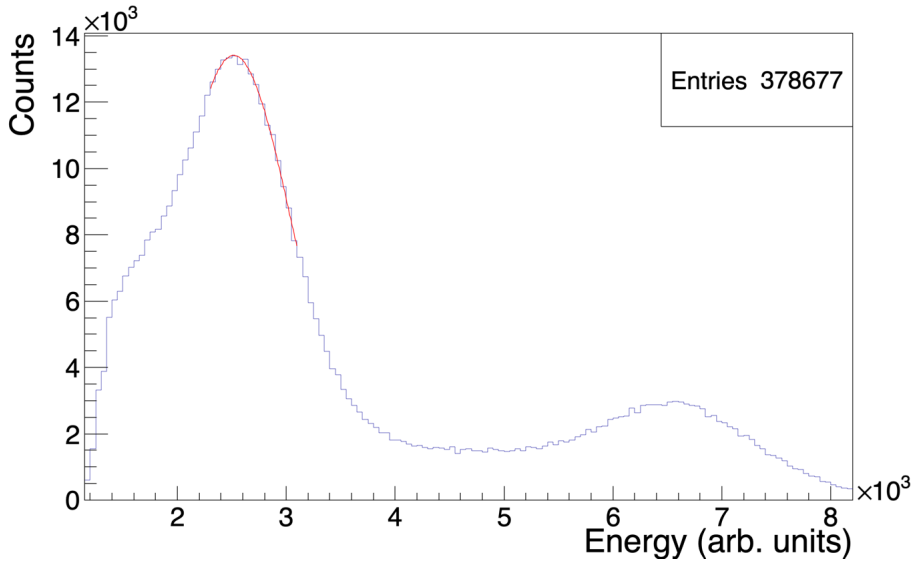

Figure 17: Fitting a peak to a Gaussian distribution using ROOT fit panel

The obtained values of the mean, standard deviation and/or FWHM, are summarized in Table 1 on the following page. The energy resolutions here were calculated using Equation 1. All of these values, alongside their errors, were tabulated for every PMT across all 3 detectors.

Detector	PMT	Photon Energy	Energy Resolution (%)	Absolute Error (%)
D1	TR	511 keV	-	-
	TL		-	-
	BR		65.387	1.603
	BL		63.800	1.199
	TR	1.274 MeV	28.689	0.242
	TL		52.593	1.669
	BR		34.522	0.447
	BL		29.456	0.274
	TR	Sum	-	-
	TL		-	-
	BR		-	-
	BL		-	-
D2	TR	511 keV	21.571	0.046
	TL		23.801	0.051
	BR		26.457	0.064
	BL		21.907	0.051
	TR	1.274 MeV	13.337	0.035
	TL		14.800	0.038
	BR		14.657	0.041
	BL		13.370	0.034
	TR	Sum	12.005	0.214
	TL		11.217	0.154
	BR		09.740	0.302
	BL		10.701	0.156
D3	TR	511 keV	51.178	0.756
	TL		45.603	0.732
	BR		23.517	0.097
	BL		25.089	0.105
	TR	1.274 MeV	27.486	0.479
	TL		20.450	0.080
	BR		14.620	0.053
	BL		15.981	0.062
	TR	Sum	-	-
	TL		-	-
	BR		11.423	0.449
	BL		-	-

Table 1: Table of Energy Resolutions for all BaF_2 Detectors and their PMTs

5 Discussion

5.1 Addressing Inconsistencies

When looking at Table 1, it is immediately apparent that not all peaks were visible in the obtained spectra. This can also be seen when looking at the various obtained spectra in Appendix B.

In relation to this, due to the relatively low energy of the 511 keV peak present in the ^{22}Na spectrum, and the fact that the same pulse detection trigger threshold was kept consistent for a given PMT, this explains why the trigger threshold was set quite low when taking measurements. This was to ensure that as many of the 511 keV photons were detected as possible. Consequently, some spectra contained a negative peak in the background, as discussed in the previous section.

Detector 1 has the worst resolutions of the three and is quite inconsistent across the four PMTs it consists of. Detector 3 has better results than Detector 1, but still has quite low resolutions compared to Detector 2. Regardless, all three detectors yielded worse resolutions than were expected, with the best obtained resolution at 511 keV being (21.571 ± 0.046)%, whereas a value of around 9.8% was expected. Noting that all detectors contained the same type of PMT and voltage dividers supplied with similar voltages and that the settings for the Trapezoidal FIR Energy Filter were consistent across all measurements taken, the inconsistency was most likely due to differences and flaws within the detectors themselves.

Before discussing these potential flaws with the detectors, it is noteworthy to mention that due to Detector 3 being within some form of a case, this could explain why the sum peak is not visible for most of its PMTs. For Detector 3, the source was placed against the casing, but since the casing was larger than the actual detector itself, this meant that there was effectively more distance between the source and the detector crystals compared to the other 2 detectors. With the source farther away, the probability of both the 511 keV and 1.274 MeV photons hitting simultaneously drastically decreases. The detector was not pushed all the way into the casing as it would have been difficult to connect wires to the PMTs, and in general it could not easily be moved within the case due to it's weight and the interior of the casing being lined with a rubbery material. However, whether considering this difference in distance or not, it can be deduced that Detector 1 was the worst performing detector and possibly has problems with the detector itself.

Two most likely explanations would be that small light leaks exist within the detector, causing unwanted photons to enter the PMTs and being converted into pulses, or that the optical seal between the detector crystal and it's corresponding PMT is not ideal, causing photons to escape and thus reducing the resolution. In order to determine the problem and attempt to resolve it, Detector 1 was taken apart.

5.1.1 Diagnosing Detector 1

Upon opening Detector 1, it was found that some PMTs were not centered on their corresponding crystals properly, with some even missing a sufficient layer of optical grease at their contact point with the crystals. In addition to this, with the crystals having a rectangular cross-section and the PMT having a circular one, the corners of the crystal are not covered by the PMT opening or even some sort of reflective material. All of these factors contribute to light loss, lowering the efficiency and resolution of the detectors. There also existed areas missing tape, potentially causing light to leak into the detector and be picked up by the PMTs. The crystal and PMT surfaces were then cleaned, with a new layer of optical grease applied, before reassembling the detector and adding tape to the areas that were missing some. Since it was found that there indeed was a problem with the seal between the PMT and the crystals, the recommended voltage of 2200V was tried once again, which ended up successfully working. This resulted in much higher output voltages in the order of magnitude of 1s of volts as opposed to the 10s of millivolts as before. Thus, the gain was reduced to the minimum value of x2 on the TFA.

A measurement from one of the fixed PMTs was then taken using the recommended input bias voltage. This was compared to a new measurement taken using the bias voltage and TFA settings previously used. The obtained spectra can be seen in the figure below.

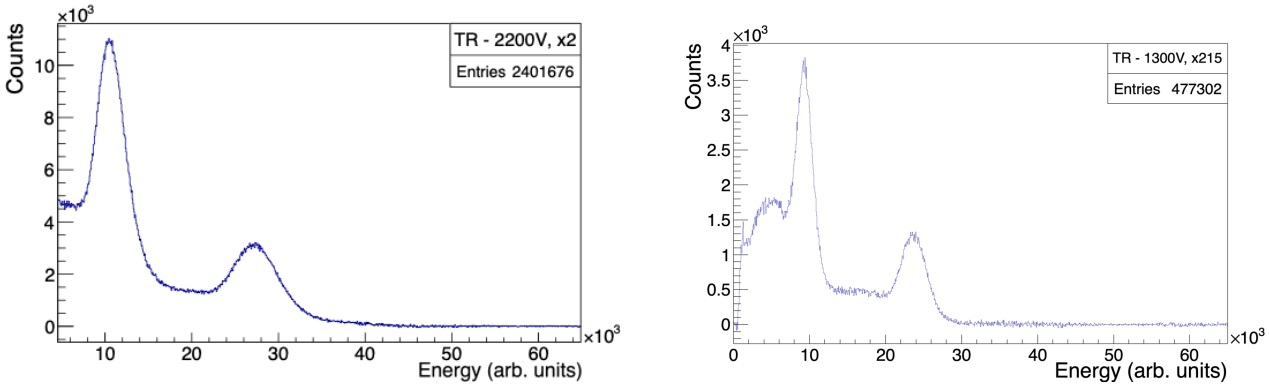

(a) Using recommended High Voltage

(b) Using previously used High Voltage

Figure 18: ^{22}Na Spectra obtained from a fixed D1 PMT

When comparing the two spectra above, it can be seen that in both cases the shape of the spectrum is comparable. However, the entry count for the recommended bias voltage is much higher. It can thus be deduced that using a higher voltage increases the amount of entries significantly, but results in roughly the same spectrum shape with a comparable resolution. This implies that after a given bias voltage for a PMT, the resolution does not vary significantly.

Since the spectrum obtained after the fix is better than those obtained before, see Appendix B, an entirely new set of measurements were taken for the now fixed Detector 1. All of the new energy

resolutions can be seen in Table 2 below.

Detector	PMT	Photon Energy	Energy Resolution (%)	Absolute Error (%)
D1 (Fixed)	TR	511 keV	24.186	0.163
	TL*		25.676	0.086
	BR		35.822	0.406
	BL		76.809	2.624
	TR	1.274 MeV	16.034	0.081
	TL*		16.081	0.044
	BR		18.262	0.054
	BL		23.537	0.089
	TR	Sum	-	-
	TL*		10.001	0.160
	BR		-	-
	BL		-	-

Table 2: Table of Energy Resolutions for Detector 1's PMTs after Fix
*** Different optical grease applied**

When comparing these new results to those originally obtained for Detector 1 in Table 1, it is immediately apparent that the resolution is now better and more consistent across the PMTs. The 511 keV peaks can now be seen for all of the PMTs, with generally better resolutions for the 1.274 MeV peak. One PMT was also able to produce a spectrum with a visible sum peak. All of the obtained spectra can be seen in Appendix C.

On another note, as mentioned in the table caption, when applying a new layer of optical grease to the PMTs, a different grease was used for one of them, namely the top left. This was done since different optical greases have different transmissibilities of photons at different wavelengths. Since the wavelengths that the greases were rated for were not specified, specifically whether UV wavelengths were included or not, it was decided to try another grease for one of the PMTs to compare the performance.

It can be seen that the fixed D1TL, having a different optical grease than the other 3 PMTs, was able to not only achieve a relatively better resolution, but it was also able to resolve a sum peak. Thus, it can be deduced that the optical grease applied to D1TL is better suited for BaF_2 crystals paired with this model of PMT.

5.1.2 D1BL Performance

Addressing the resolutions obtained by D1BL, the performance of this PMT is still not optimal, even after the fix. The obtained spectrum for it can be seen below.

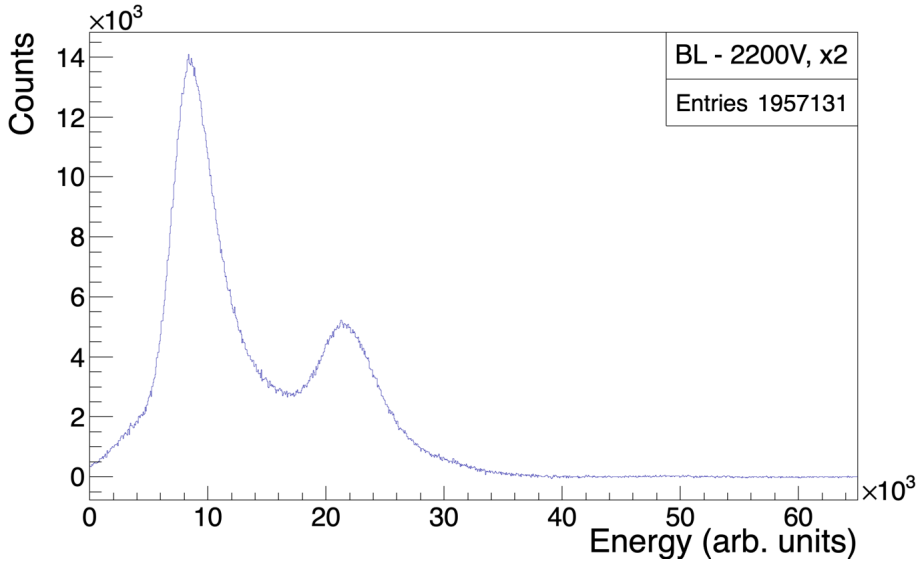

Figure 19: Background-subtracted energy spectra for a ^{22}Na source obtained by fixed D1BL

From the figure, it can be seen that the 511 keV peak is blended into the background. This is noticeable as the peak is not exactly Gaussian, but is wider on the right side than the left side. Since this is at the functional voltage, this means that the PMT itself might be faulty. Further proof for this is that when using the old bias voltage and varying the gain settings, the following spectra are obtained.

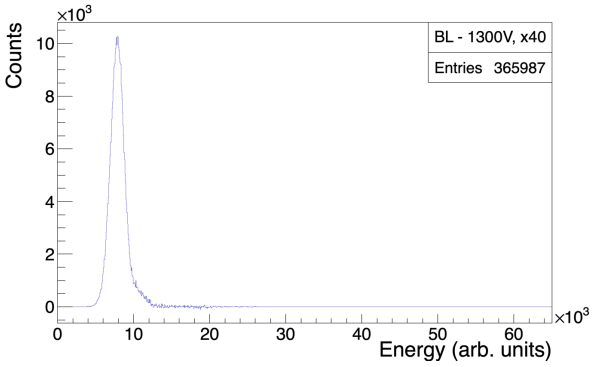

(a) Original Bias Voltage, Low Gain

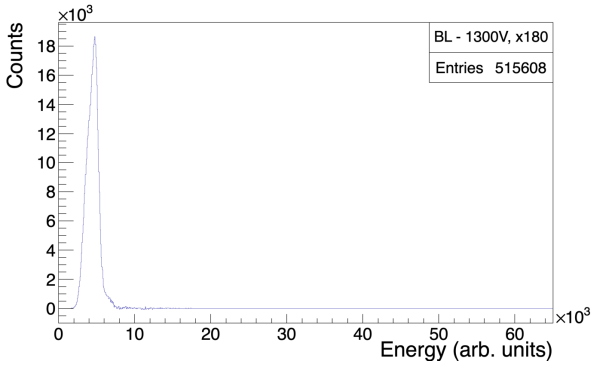

(b) Original Bias Voltage, High Gain

Figure 20: Background-subtracted energy spectra for a ^{22}Na source obtained by fixed D1BL using original input bias voltage

In both cases, the internal gain of the PMT at the input bias voltage of 1300V is not high enough to amplify the pulses outside of the order of magnitude of the electronic noise. Thus, adding more external gain would not improve the spectrum. This paired with the fact that the 511 keV peak is still not able to be amplified out of the electronic noise for the detector at the recommended functional voltage, implies that the PMT itself has low internal gain, or that the voltage divider base is faulty. This means that the PMT might have degraded over time, reducing the internal gain and overall performance. Thus, replacing the PMT will probably be necessary if this detector were to be used in a proper experimental setup.

5.1.3 Takeaway

Since, in the end, Detector 1's PMTs could operate at the recommended functional voltage, this implies the same would apply for the other detectors as well. Additionally, since the pulse amplitude also increased, this would allow for the minimizing or omission of amplification of the signal with the Timing Filter Amp, but the integration would still be necessary as the fast decay time remains constant and is characteristic to the BaF_2 crystal. Regardless, the obtained results are still representative of the performance of the detector as the same spectrum shape was observed whether using the recommended bias voltage, or the voltage settings that were used originally.

The reason this was discovered so late is that the operating voltage was decided based on the first detector being used, being Detector 1, which happened to be the faulty detector. Settings were intended to be kept consistent when taking measurements with the other 2 detectors afterwards. Not operating with the correct operating voltage could also explain why some PMTs were not able to fully resolve the 511 keV peak, as can be seen in Figure 15b for example. In a lot of the histograms, the 511 keV peak was blending into the background, causing the resolution to become worse. Unfortunately, even after the fix, this remained the case for D1BL.

It can thus be concluded that Detector 1 contained an imperfect optical seal, with some PMTs missing sufficient optical grease, and there were light leaks that were subsequently addressed via taping the areas accordingly. However, after fixing the detector, the resolutions obtained are still not comparable to those achieved with Detector 2, and not all detectors were able to resolve the sum peak. This might be due to the corners of the detector crystals not being covered by the PMT or a reflective material, still resulting in light loss, as previously mentioned. Additionally, it is noteworthy to mention that the PMTs were not necessarily placed back into the same places as before, and thus the D1TR of the fixed detector doesn't necessarily correlate to the TR PMT before the fix.

The last take away is that the type of optical grease matters. D1TL, having a different optical grease than the other three PMTs, was able to resolve the sum peak whereas the others couldn't.

5.2 Resolution-Energy Relationship

Even with an improvement in energy resolution for Detector 1, the resolution was still not sufficient enough to resolve the ^{60}Co peaks. Regardless, there are still 3 values that can be used to plot a relationship between the energy resolution and the incident photon energy for some of the PMTs across the detectors. Two values would not suffice for observing a proper relationship described by a non-linear function, so only data from PMTs that were able to resolve all three ^{22}Na peaks will be fitted according to Equation 6. An example of a plot of the resolutions fitted by the equation can be seen below, where the rest can be found in Appendix D.

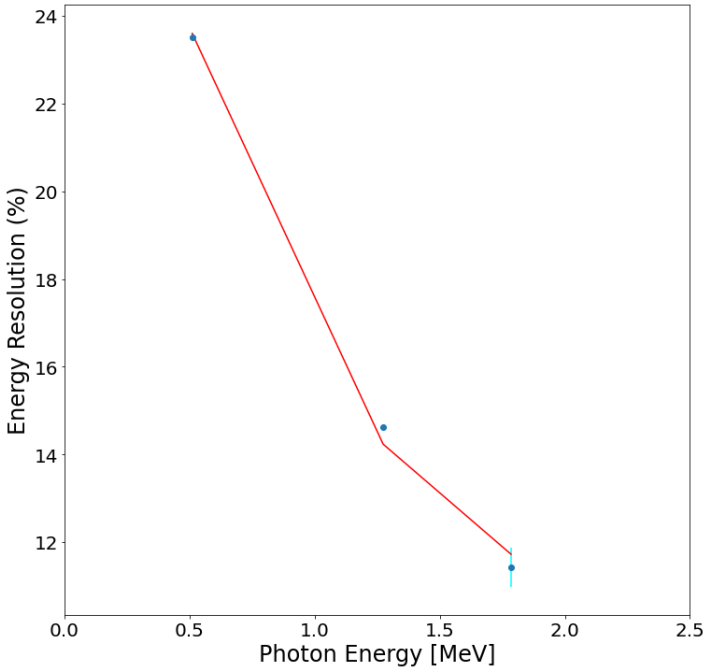

Figure 21: Energy Resolution and Photon Energy Relationship for D3BR

In the plot above it can be seen that the fit does not fall within all of the error bars of the individual points. This is because these obtained error bars correspond to uncertainties within the Gaussian fit itself when determining the FWHM and mean values. The fitting method used for the spectra corresponding to these plots is the method used in Figure 16. This method was used as the spectra were clear enough where the background and Compton effects could be properly distinguished from the peaks. As previously mentioned, this background behaviour was fitted using a third order polynomial. However, this is of course just an approximation, where the true behaviour is more complicated. Thus, this approximation comes with it's own limitations and uncertainties, which would explain why the fit does not pass through all of the points' error bars. Additionally, only three data points were used for this fitting. If the ^{60}Co peaks were resolved, this would result in 5 data points and thus a more accurate fit.

The fit parameters obtained when fitting all of these energy resolution values to the corresponding incident photon energy can be seen in Table 3 below.

Detector & PMT	Parameter C (Scaling Factor)	Parameter D (Offset)
D1TL (Fixed)	22.627	-5.626
D2TR	15.075	0.395
D2TL	18.855	-2.459
D2BR	24.965	-8.291
D2BL	17.070	-1.933
D3BR	18.248	-1.930

Table 3: Table of Obtained Fit Parameters

It can be seen that in all cases the resolution does indeed follow the proportionality indicated in Equation 5. However, how true they follow the proportionality, indicated by the offset parameter, varies quite a bit.

As discussed in Section 2.4.1, the closer the fit parameter D is to 0, the more accurate the fit and the more accurately the obtained energy resolutions obey the proportionality. Thus, it can be seen that the approach used was sufficient enough for most PMTs due to relatively low values of D obtained. For example, the resolutions obtained are in the order of magnitude of 10s, whereas the offset parameter D is in the order of magnitude of 1s. This means that the problem of observing higher percentages of energy resolution generally lies within the detectors themselves as opposed to the approach used. This can be due to poor design, as was observed within Detector 1, or due to faults or degradation of the PMTs.

For the PMTs with offset parameters farther away from 0, as is the case for D1TL and D2BR, this is most likely due to how the background was fit when fitting the function. Once again, fitting the background to a third-order polynomial is simply an approximation coming with its own uncertainties. However, some human error might be a contributor to the extreme values for D1TL and D2BR since the fit areas are decided manually.

6 Conclusion

6.1 Summary of Findings

Overall, this project was concerned with characterizing how suitable BaF_2 detectors would be in the context of neutron cross-section determination, but due to limitations in time, the goal was focused more on probing what exact energy resolutions can be expected by these detectors. Undoped BaF_2 scintillator detectors, as compared to HPGe semiconductor detectors, have worse energy resolutions, with a resolution of $\sim 10\%$ at 511 keV, compared to a resolution of $\sim 0.2\%$ achievable by HPGe.

Using an ORTEC 474 Timing Filter Amplifier to amplify and integrate the pulses as well as the Trapezoidal FIR Energy Filter approach to filter and store the data, spectra were plotted for radioactive sources of known photon energies. The radioactive sources were used in order to determine the resolutions via their produced energy spectra. The sources are a ^{60}Co source, with peaks at energies of 1.173 and 1.332 MeV, and a ^{22}Na source, with peaks at energies of 511 keV and 1.274 MeV. Unfortunately, it was found that the detectors weren't able to resolve the ^{60}Co peaks, so only the ^{22}Na were taken into consideration.

The expected energy resolution at the photon energy of 511 keV was $\sim 9.8\%$, but the best achieved resolution at this energy was $(21.571 \pm 0.046)\%$. Additionally, a resolution of around $\sim 6.4\%$ was expected for the 1.334 MeV peak of ^{60}Co. However, since none of the detectors were able to resolve the ^{60}Co peaks, with both being close in energy, this value can be compared to the comparable peak of 1.274 MeV originating from the ^{22}Na source. The best obtained resolution at this photon energy was $(13.337 \pm 0.035)\%$, obtained by the same PMT that yielded the best resolution at 511 keV. Once again, this is worse than the expected resolution by around a factor of 2. This discrepancy in resolution may be due to design flaws of the detectors themselves, or due to degraded or faulty PMTs/voltage dividers.

This was identified to be the case for one detector, namely the one that all of the data collection settings were based upon, when it was found to be faulty. Once light leaks in the detector were addressed, and the PMTs were fixed and with new optical grease applied, the resolution of this detector improved. However, it was still not to the extent that was expected. This might be due to a design flaw within the detector itself where photons can be lost at the corners of the crystals, being square in shape, when the PMTs have a circular cross-section. As for the other detectors, especially detector 2 having performed the best and most consistently, a flaw like this might also be the limiting factor for the resolution.

Further proof that the discrepancy arises from the detectors themselves and not the data collection approach can be seen with the fits obtained when plotting the obtained energy resolutions against the corresponding incident photon energies. The relationship follows an inverse square root proportionality to the photon energy, but a scaling factor and offset parameter term were introduced to properly observe the fitting behaviour and assess the reliability of the obtained resolution values. For the PMTs that were able to resolve all 3 peaks of ^{22}Na: the 511 keV, 1.274 MeV, and sum peaks, this relationship was plotted with offset parameters generally ranging between $\approx 1-2\%$, with the best obtained value being 0.395. In the context of the energy resolutions being of the order of magnitude of 10s, these offset values are relatively close to 0. This means that the resolutions obtained act quite as expected, further justifying the reliability of the experimental approach used in this thesis. There exist, however, two cases where the offset parameter was significant larger. This is probably due to the accuracy of the chosen fit function used to predict the background behaviour, being a third-order polynomial approximation, when analyzing the spectra to calculate the energy resolutions.

All in all, it can be concluded that, in terms of purely energy resolution at least, the undoped BaF_2 scintillator detectors would not necessarily be a worthy investment when it comes to upgrading the current GAINS spectrometer at the GELINA facility.

6.2 Future Work

Once again, due to limited time, only the energy resolution of the BaF_2 detectors was characterized. However, it would be very relevant to experimentally investigate the efficiency of these detectors, as this is where BaF_2 has the upper hand over HPGe detectors, which are currently present in the GAINS spectrometer. If a significantly higher efficiency is achievable for BaF_2 detectors, it can be said that they would be a worthy implementation to the current GAINS spectrometer. This would allow for more precision and/or accuracy regarding the yield of photons for a given neutron inelastic scattering reaction.

References

[1] A. Olacel, C. Borcea, M. Boromiza, *et al.*, "The past and the future of the gains spectrometer @ gelina," *EPJ Web of Conferences*, vol. 284, May 2023. DOI: 10.1051/epjconf/202328401007.

[2] "Safety of nuclear reactors - world nuclear association." (), [Online]. Available: https://world-nuclear.org/information-library/safety-and-security/safety-of-plants/safety-of-nuclear-power-reactors.aspx. (accessed: 20-06-2023).

[3] A. Negret, C. Borcea, P. Dessagne, *et al.*, "The limits of the gains spectrometer," *Nuclear Data Sheets*, vol. 119, pp. 179–182, 2014, ISSN: 0090-3752. DOI: https://doi.org/10.1016/j.nds.2014.08.050. [Online]. Available: https://www.sciencedirect.com/science/article/pii/S0090375214005845.

[4] I. Hossain, N. Sharip, and K. K. Viswanathan, "Efficiency and resolution of hpge and nai(tl) detectors using gamma-ray spectroscopy," *Sci. Res. Essays*, vol. 7, Jan. 2012.

[5] G. Kalsulkar, "Characterization and optimization of csi and nai(tl) detectors for gains," *Master's Thesis*, Jun. 2023.

[6] U. Ackermann, W. Egger, P. Sperr, and G. Dollinger, "Time- and energy-resolution measurements of baf2, bc-418, lyso and cebr3 scintillators," *Nuclear Instruments and Methods in Physics Research Section A: Accelerators, Spectrometers, Detectors and Associated Equipment*, vol. 786, pp. 5–11, 2015, ISSN: 0168-9002. DOI: https://doi.org/10.1016/j.nima.2015.03.016. [Online]. Available: https://www.sciencedirect.com/science/article/pii/S0168900215003101.

[7] K. Wisshak, K. Guber, and F. Käppeler, "Gamma-ray spectroscopy with a cooled barium fluoride crystal," *Nuclear Instruments and Methods in Physics Research Section A: Accelerators, Spectrometers, Detectors and Associated Equipment*, vol. 259, no. 3, pp. 583–585, 1987, ISSN: 0168-9002. DOI: https://doi.org/10.1016/0168-9002(87)90844-8. [Online]. Available: https://www.sciencedirect.com/science/article/pii/0168900287908448.

[8] S. Tavernier, *Experimental Techniques in Nuclear and Particle Physics*. Oxford University Press, 2010, ISBN: 978-3-642-00829-0, 978-3-642-00828-3. DOI: 10.1007/978-3-642-00829-0.

[9] U. Ackermann, W. Egger, P. Sperr, and G. Dollinger, "Time- and energy-resolution measurements of baf2, bc-418, lyso and cebr3 scintillators," *Nuclear Instruments and Methods in Physics Research Section A Accelerators Spectrometers Detectors and Associated Equipment*, vol. 786, Jun. 2015. DOI: 10.1016/j.nima.2015.03.016.

[10] M. Kavatsyuk, *Lecture notes on scintillation detectors*, 2023.

[11] G. F. Knoll, *Radiation Detection and Measurement, 3rd ed.* 3rd edition. New York: John Wiley and Sons, 2000, ISBN: 978-0-471-07338-3, 978-0-471-07338-3.

[12] I. Ukaegbu and K. Gamage, "A model for remote depth estimation of buried radioactive wastes using cdznte detector," *Sensors*, vol. 18, p. 1612, May 2018. DOI: 10.3390/s18051612.

[13] F. Krauss, *Lecture notes: Detector & statistics in a nutshell*.

[14] "Energy resolution in gamma spectrometry." (), [Online]. Available: https://physicsopenlab.org/2016/02/07/energy-resolution-in-gamma-spectrometry/. (accessed: 11-07-2023).

[15] Photonis, *Photomultiplier Tubes Catalogue*. France.

[16] S. I. S. GmbH, *SIS3316 16 Channel VME Digitizer User Manual*. Hamburg, Germany, 2020.

[17] K. Gunoglu and S. Arda, "Detection efficiency of nai(tl) detector in 511–1332 kev energy range," *Science and Technology of Nuclear Installations*, vol. 2014, pp. 1–5, Mar. 2014. DOI: 10.1155/2014/186798.

[18] A. Qureshi, A. Sultan, A. Rashid, *et al.*, "Geological and radiological studies of the mount arafat, mekkah, saudi arabia," *Journal of Radioanalytical and Nuclear Chemistry*, vol. 293, Sep. 2012. DOI: 10.1007/s10967-012-1776-0.

Appendix

A Obtained ^{60}Co Spectra

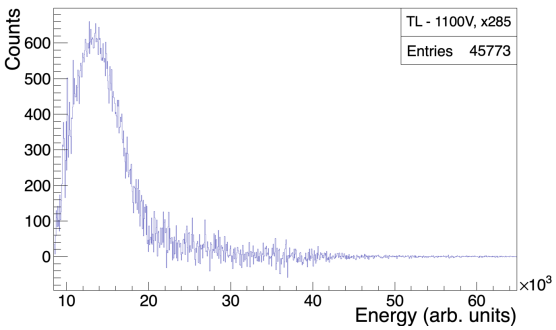

(a) TL

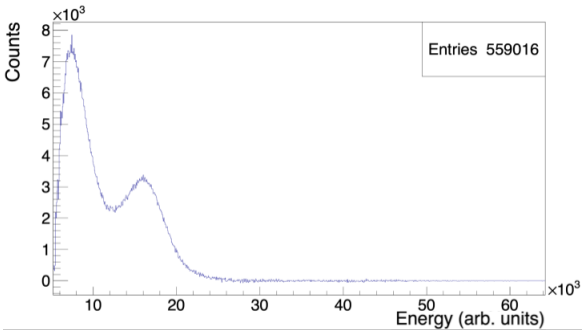

(b) TR

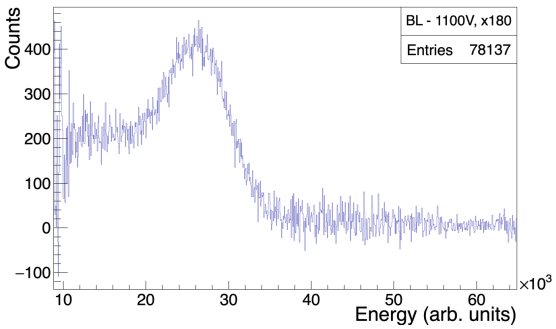

(c) BL

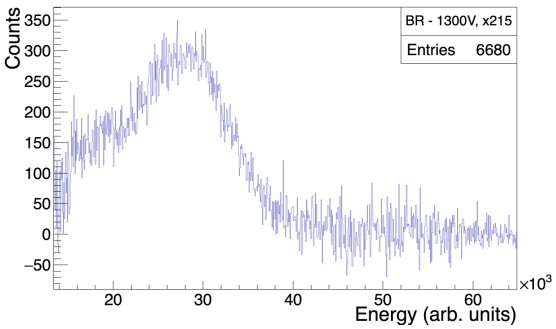

(d) BR

Figure 22: Background-subtracted energy spectra for a ^{60}Co source using Detector 1

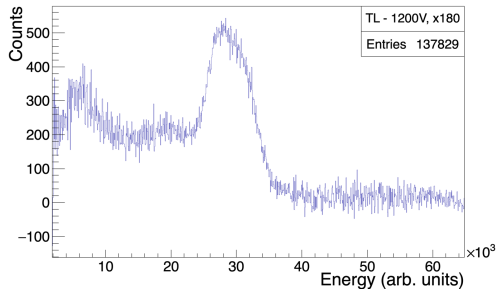

(a) TL

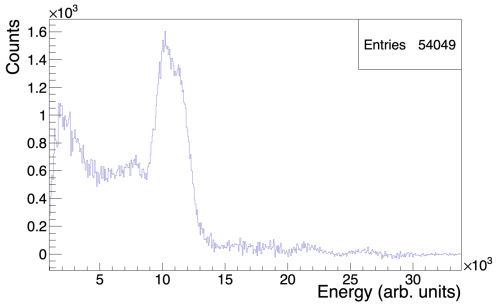

(b) TR

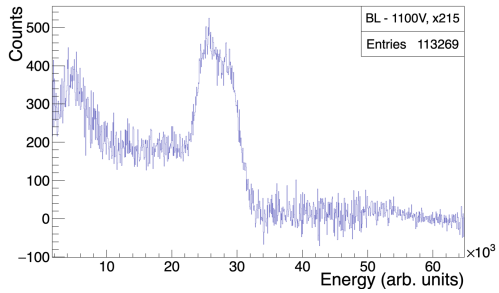

(c) BL

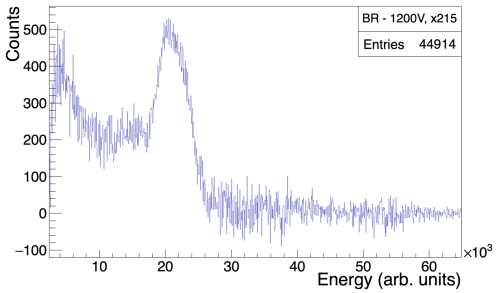

(d) BR

Figure 23: Background-subtracted energy spectra for a ^{60}Co source using Detector 2

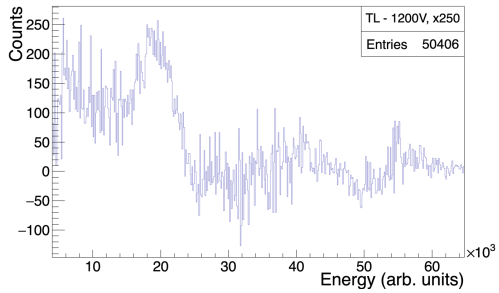

(a) TL

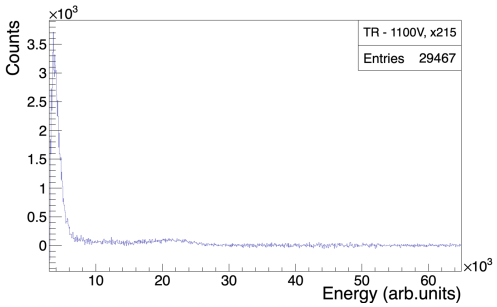

(b) TR

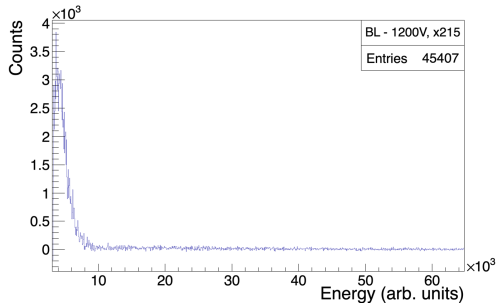

(c) BL

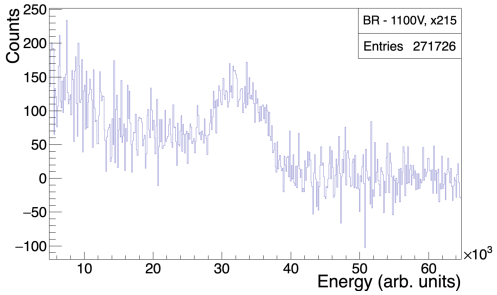

(d) BR

Figure 24: Background-subtracted energy spectra for a ^{60}Co source using Detector 3

B Obtained ^{22}Na Spectra

The obtained ^{22}Na source spectra, with the background subtracted, for the 4 PMTs of all 3 detectors can be seen in the following figures.

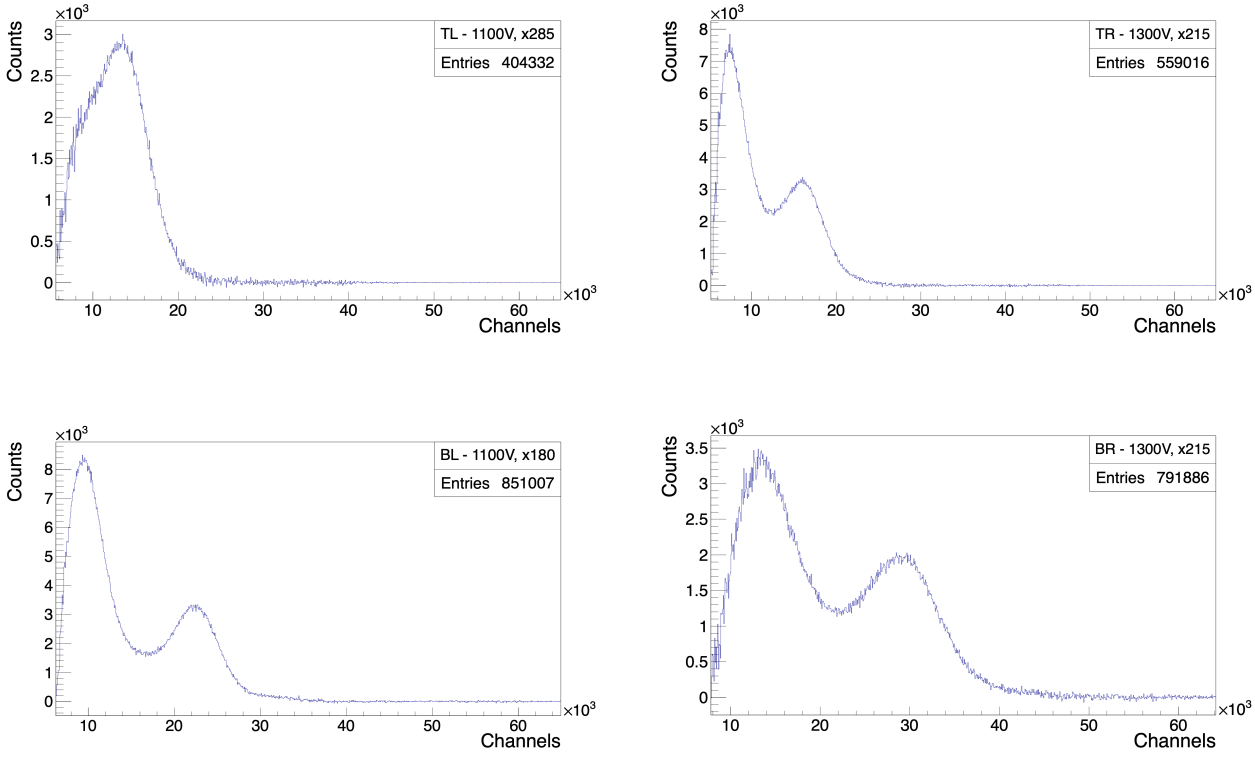

Figure 25: Background-subtracted energy spectra for a ^{22}Na source using Detector 1

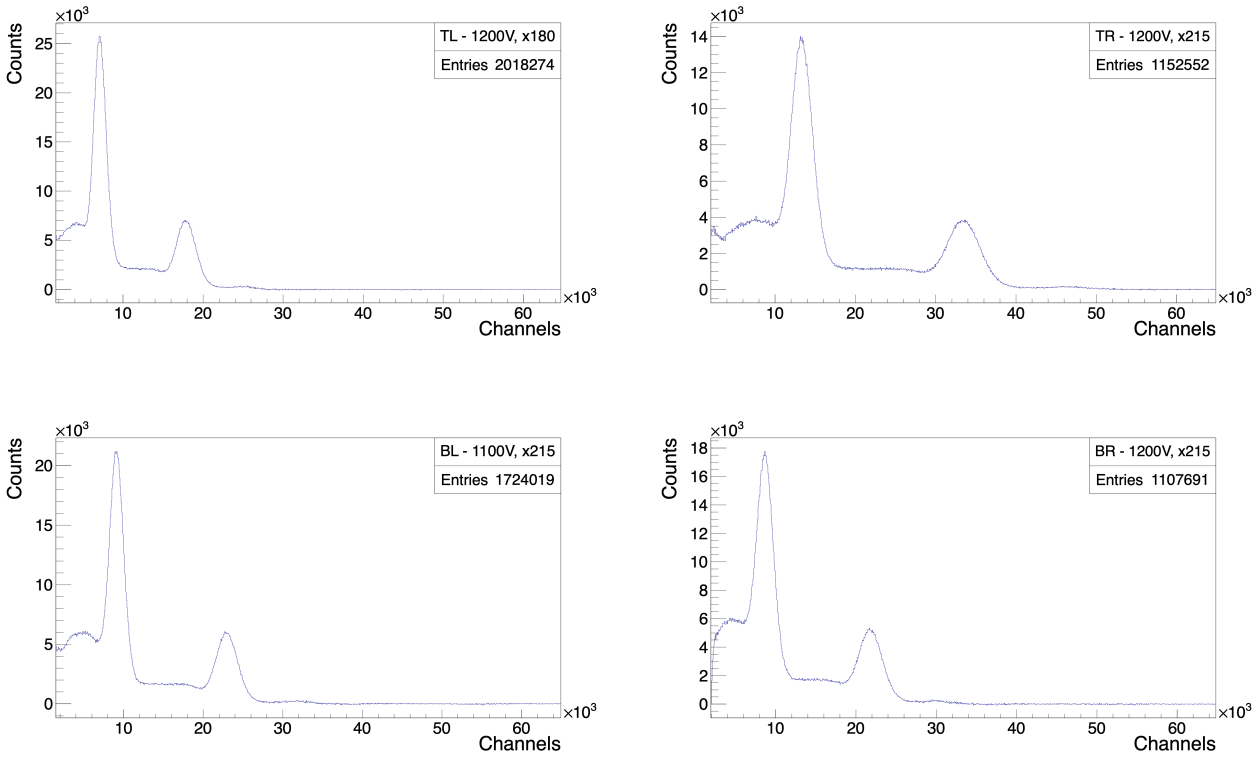

Figure 26: Obtained Energy spectra for a ^{22}Na source using Detector 2

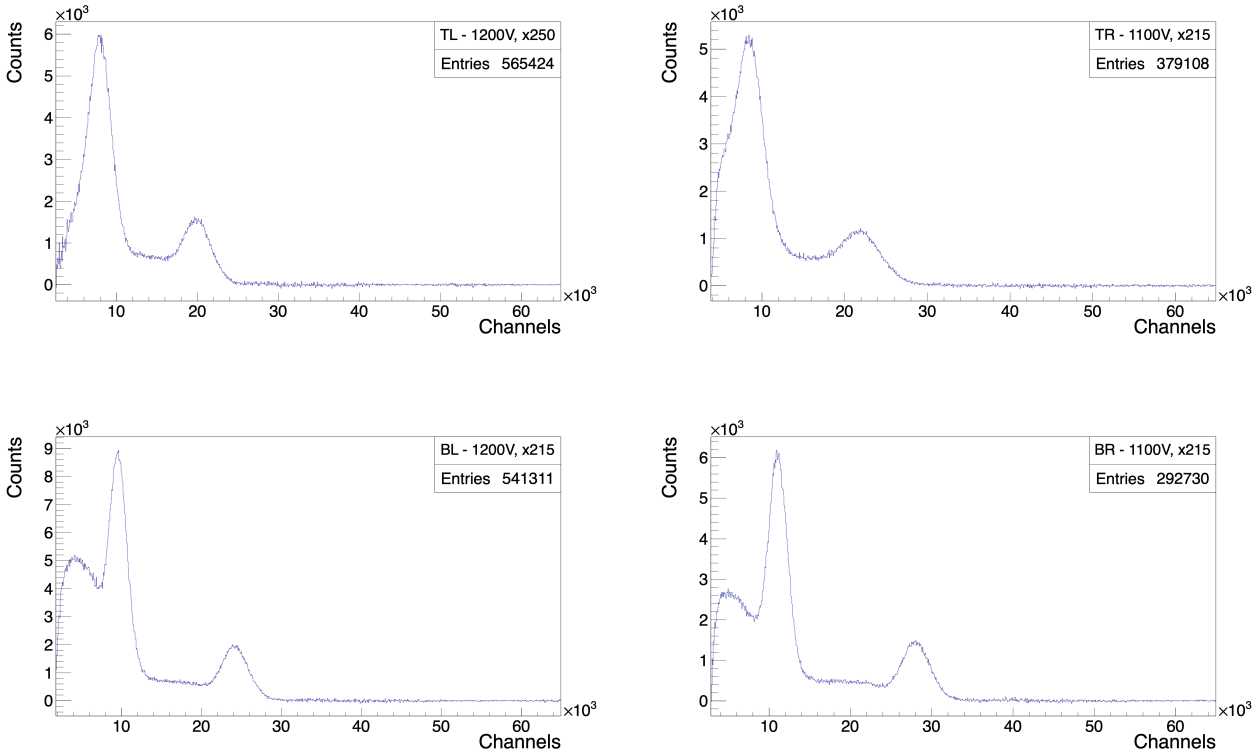

Figure 27: Obtained Energy spectra for a ^{22}Na source using Detector 3

C Obtained ^{22}Na Spectra for Fixed Detector 1

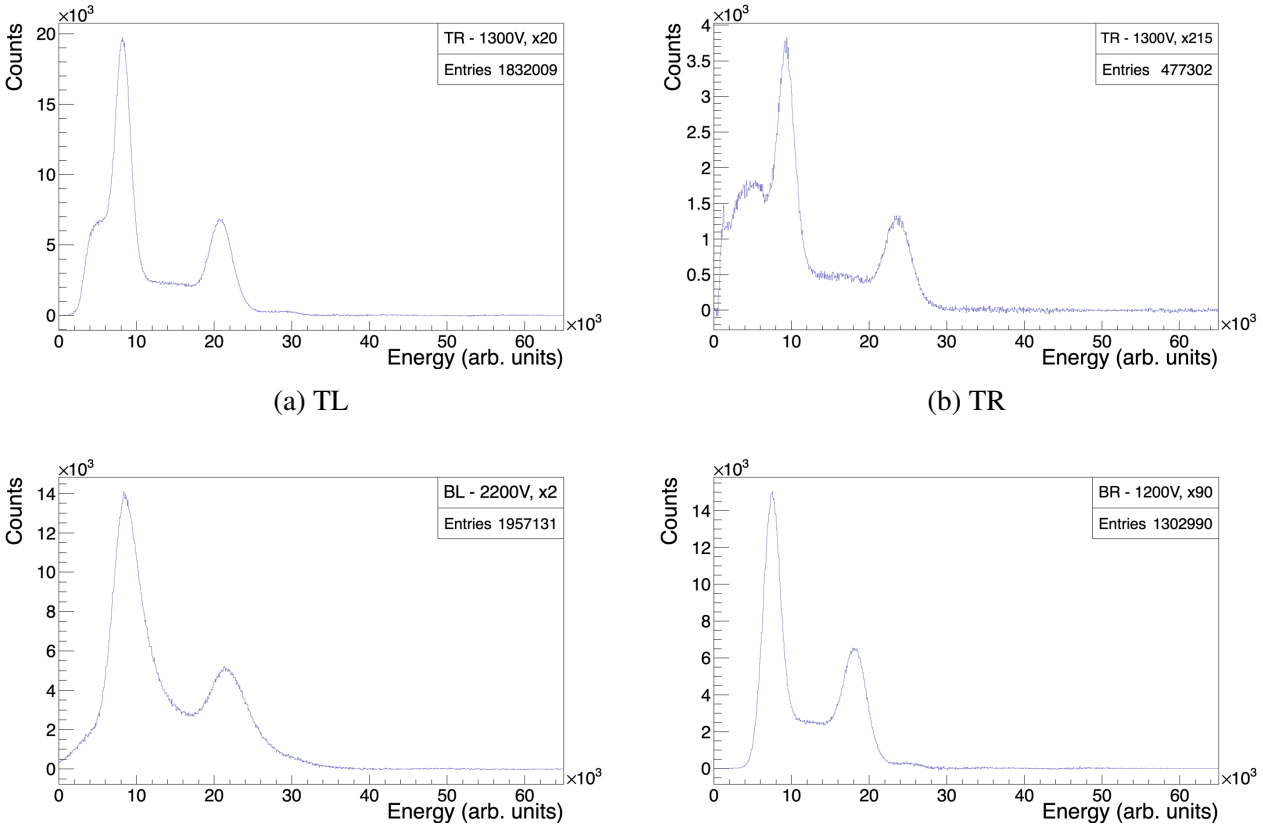

(a) TL

(b) TR

(c) BR

(d) BL

Figure 28: Background-subtracted energy spectra for a ^{22}Na source for the fixed Detector 1

D Energy Resolution vs Photon Energy Plots

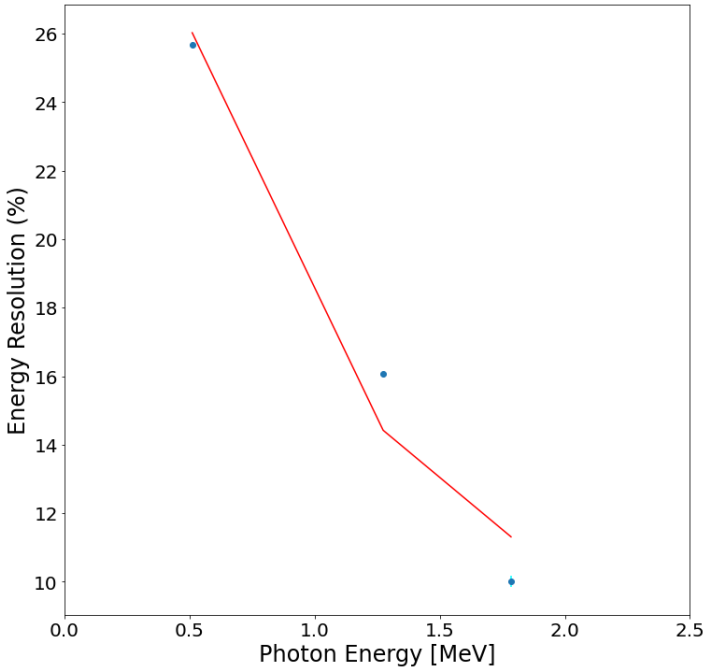

Figure 29: Energy Resolution and Photon Energy Relationship for D1TL

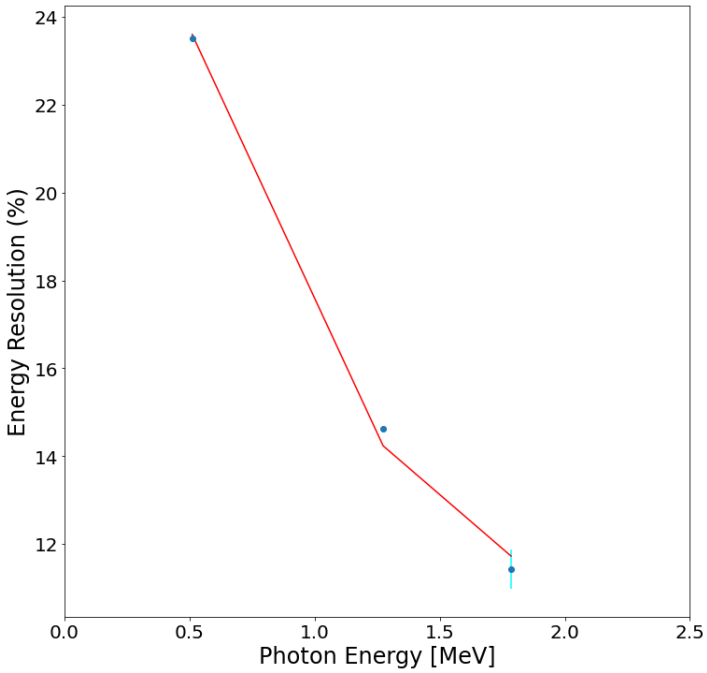

Figure 30: Energy Resolution and Photon Energy Relationship for D3BR

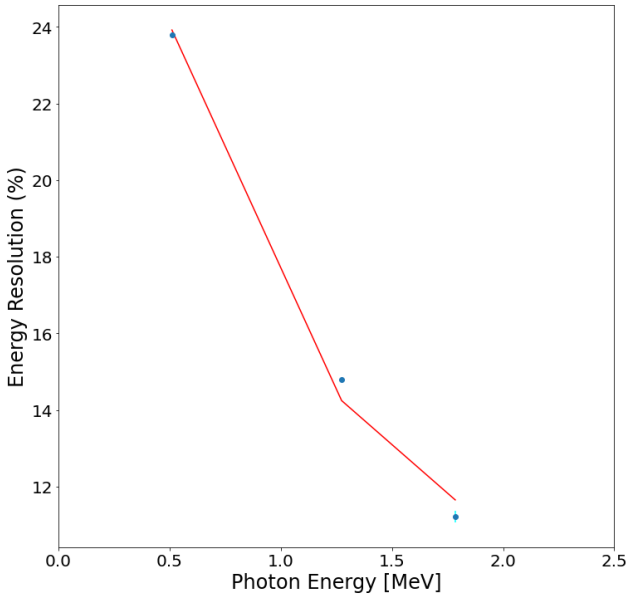

(a) TL

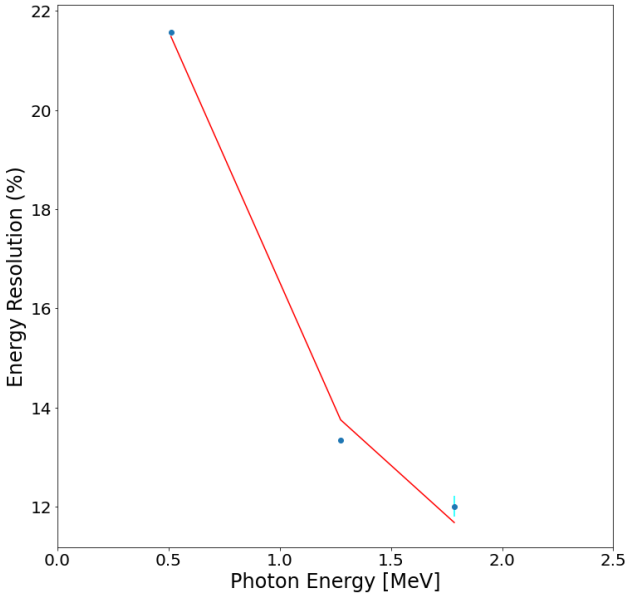

(b) TR

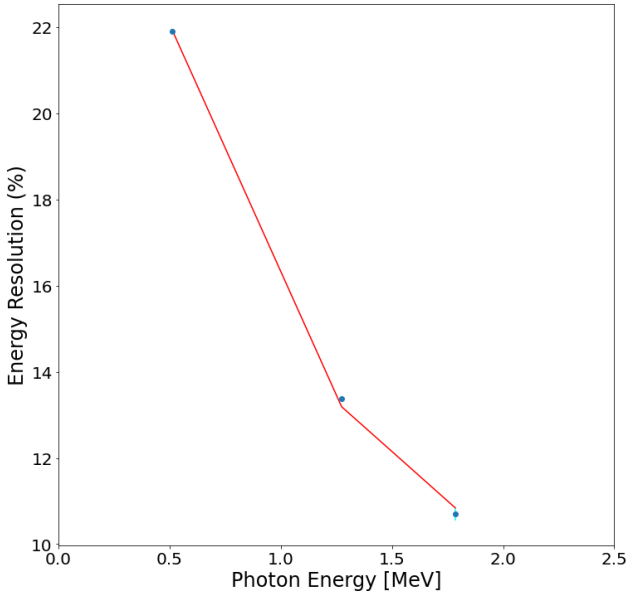

(c) BL

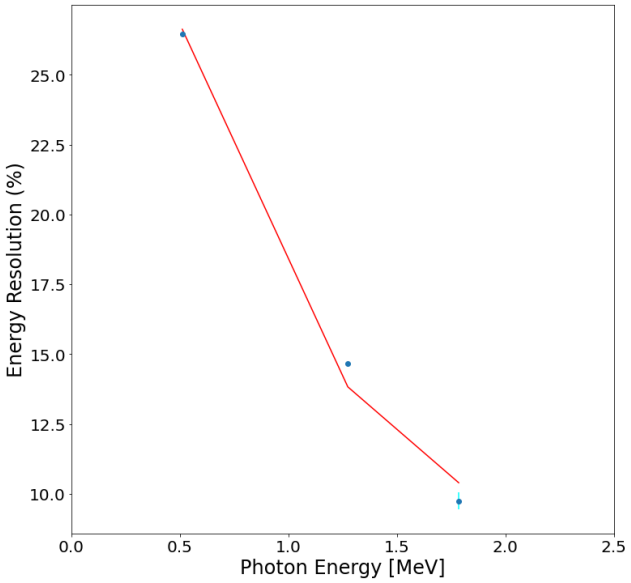

(d) BR

Figure 31: Energy Resolution and Photon Energy Relationship for D2